Enhanced Modulation for the Single-Stage Three-Phase Quad-Active-Bridge AC-DC converter

Chavez Daniel[1,2] , Sal y Rosas Damian[2], Cousineau Marc[1]
[1]LAPLACE, Université de Toulouse, CNRS, INPT, UPS, Toulouse, France, [2]LAAS-CNRS, Université of Toulouse, 31031 Toulouse, France

ABSTRACT – This paper proposes an enhanced modulation for the isolated and bidirectional single-stage three-phase Quad-Active-Bridge (QAB) AC-DC converter. In the QAB AC-DC converter, a DC OFFSET is controlled at the neutral point, allowing grid voltages to be modulated using unipolar voltage switches. In the proposed modulation, the offset grid voltages are modulated by a symmetrical duty ratio whose angle changes according to the instantaneous grid frequency, whereas the DC source is modulated by a 50% symmetrical duty ratio (DR) and a phase-shift (PS) to control the bidirectional power transfer. Hence, the command signals can be easily calculated. Converter design, simulation, and experimental results are presented. Grid currents with very low THD (2.8 %) are obtained in open-loop operation.

Keywords— AC-DC converters, single-stage, bidirectional, isolated, Quad-Active-Bridge

1. INTRODUCTION

Single-stage (SS) three-phase (3P) AC-DC converters facilitate bidirectional power flow and galvanic isolation while also offering superior performance compared to conventional two-stage AC-DC converters. The most widely used SS 3P AC-DC converters are illustrated in Fig. 1. These converters provide advantages such as reduced volume, improved efficiency, and longer lifetime [1]. However, the main drawback is the complexity of the modulation techniques used.

For example, the converter shown in Fig. 1a is composed of three independent SS single-phase AC-DC converters. Each AC-DC converter integrates a low-frequency rectifier (LFR) cascaded with a DAB DC-DC converter, which is modulated using a fixed or time-variant switching frequency [2]-[5]. Note that many switches are required, which decreases the converter efficiency and increases the converter price.

In contrast, the SS 3P DAB AC-DC converter in Fig. 1b [6] features fewer switches and incorporates only one high-frequency (HF) transformer, increasing the converter efficiency. However, the use of bipolar voltage switches in the matrix converter for grid modulation introduces a high complexity, and switch protection is also required [3].

Alternatively, the Quad-Active-Bridge (QAB) AC-DC converter shown in Fig. 1c [7] uses fewer unipolar voltage switches thanks to the offset added to the grid voltages by means of controlling the DC voltage V_{OFF} in the capacitor c_f series-connected in the grid neutral point. Hence, the converter price can be reduced. However, similarly to the DAB AC-DC converter, it requires a complex modulation, presenting significant challenges in calculating the phase-shift angles required to control the bidirectional power transfer between the grid and the DC-source. Therefore, novel modulations must be developed to promote its usability.

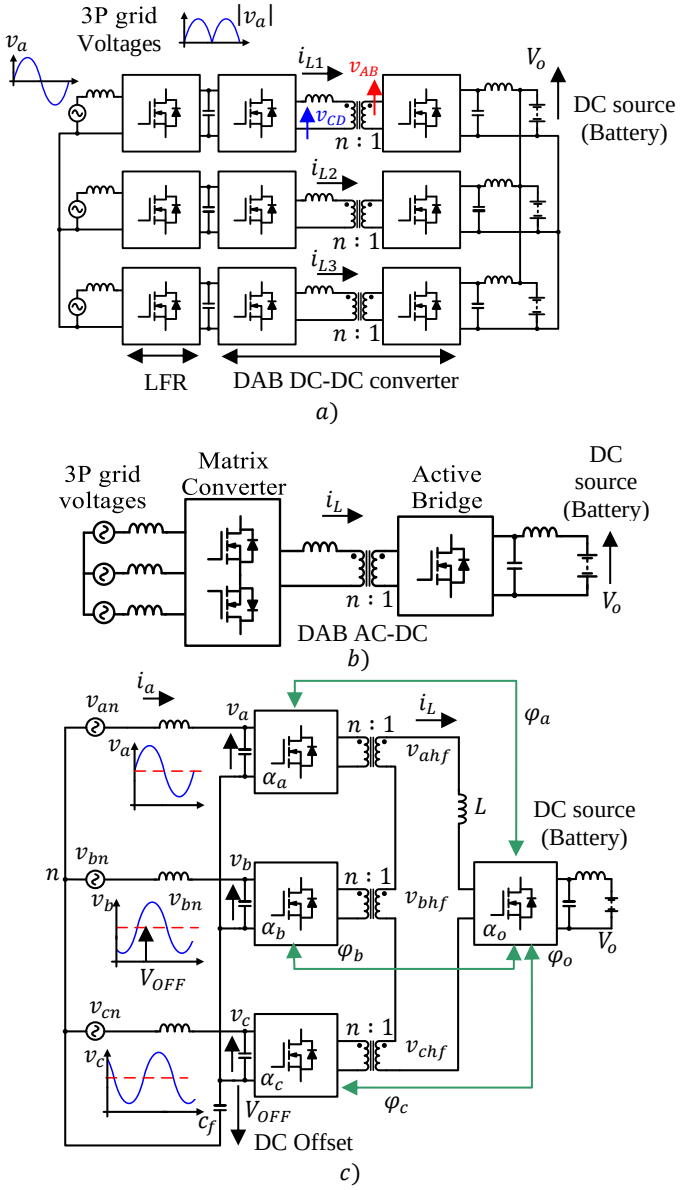

Fig. 1. SS 3P AC-DC converters a) Modular LFR cascaded to DAB single-phase AC-DC converters) b) DAB AC-DC c) QAB AC-DC converter

This paper proposes a simpler modulation for the QAB AC-DC converter. With the aim of highlighting the novelty of the proposed modulation, the existing modulations for DAB and QAB AC-DC converters are detailed below.

2. EXISTING MODULATION FOR MODULAR DAB AND QAB AC-DC

This section presents the modulation strategies used in topologies using unipolar voltage switches, as depicted in Fig. 1a and Fig. 1c, respectively. For this purpose, the 3P grid voltages are defined by:

$$\begin{cases} v_{an} = V_m sin(\omega_g t); \\ v_{bn} = V_m sin\left(\omega_g t - \frac{2\pi}{3}\right); \\ v_{cn} = V_m sin\left(\omega_g t + \frac{2\pi}{3}\right); \end{cases} \quad (1)$$

whereas the corresponding 3P grid currents are given by (2).

$$\begin{cases} i_a = I_m sin(\omega_g t); \\ i_b = I_m sin\left(\omega_g t - \frac{2\pi}{3}\right); \\ i_c = I_m sin\left(\omega_g t + \frac{2\pi}{3}\right); \end{cases} \quad (2)$$

where V_m and I_m are the amplitudes of grid voltages and currents, respectively, and ω_g represents the grid frequency.

A. Modulation for modular DAB AC-DC converters

The inner-mode and outer-mode modulations, introduced in [8] for DAB DC-DC converters. Both modulations are illustrated in Fig. 2.

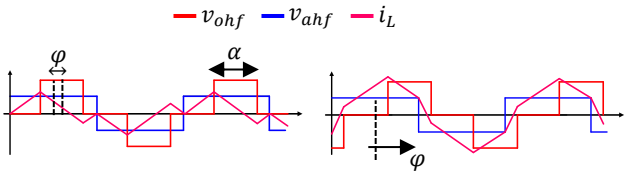

(a) Inner-mode (b) Outer-mode

Fig. 2. Modulation modes in SS DAB AC-AC converter: (a) Inner (b) Outer

Note that the inner mode occurs when v_{ohf} (the modulated battery voltage) is fully contained within v_{ahf} (the modulated grid voltage). Therefore, the PS angle φ must satisfy the following constraint $|\varphi| < \varphi_B$, where φ_B denotes the bounding phase-shift defined by:

$$\varphi_B = \frac{T_s}{4} - \frac{\alpha}{2} \quad (3)$$

where T_s is the switching period and α the DR (see Fig. 2). The inner-mode modulation for SS DAB AC-DC was introduced in [2], where the average current $\langle i_a \rangle$ is given by (19).

$$\langle i_a \rangle = \frac{nV_o}{4Lf_s}\delta d \quad (4)$$

being n the turns-ratio relationship of the High Frequency (HF) transformer, V_o is the battery voltage, L is the HF inductance, f_s is the switching frequency, which takes a constant value. The parameters δ and d are associated through the relations $\delta = 4\varphi f_s$ and $d = 2\alpha f_s$. Note in (4) that $\langle i_a \rangle$ is linearly dependent on δ and d which are non-dimensional parameters. Hence, the command signals for inner mode modulation are given by:

$$\begin{cases} d = \hat{d} \times sin(\omega_g t) \\ |\delta| < 1 - d \end{cases} \quad (5)$$

where d varies at low frequency according to ω_g, being $\hat{d}$ the amplitude. Then, according to (4), the parameter d controls the time variations of $\langle i_a \rangle$ whereas δ controls its amplitude. However, the main constraint of this modulation is the high resolution required for practical implementation and the high HF current resulting.

On the other hand, the outer-mode represents the complementary condition of inner-mode, it means $|\varphi| > \varphi_B$ [8], where φ_B is given by (3). Hence, the outer-mode modulation for SS DAB AC-DC was introduced in [3], where the average grid current $\langle i_a \rangle$ is given by:

$$\langle i_a \rangle = \frac{nV_o}{Lf_{s\_var}}\varphi \quad (6)$$

where f_s is time-variant according to (7), with the aim of obtaining a linear relationship between $\langle i_a \rangle$ and φ.

$$f_s = f_{s\_var}(1 - 2\varphi) \quad (7)$$

Therefore, the command signals are given by:

$$\begin{cases} \varphi = \hat{\varphi} \times sin(\omega_g t) \\ \alpha = 2\varphi \end{cases} \quad (8)$$

Note that, according to (8), φ controls the amplitude and the low frequency variations of $\langle i_a \rangle$. However, the main limitation of this modulation lies in the high complexity associated with varying f_s according to (7). This results in increased design effort for the HF inductor, the HF transformer, and the EMI filters. Similar approaches for outer mode have been proposed in [4][5].

B. Modulation for the QAB AC-DC converter

In the QAB AC-DC converter (see Fig. 1c), the voltage V_{oFF} across the capacitor C_f is regulated to maintain a constant DC value greater than the peak grid voltage V_m. Therefore, the QAB voltage inputs on the AC side are expressed by:

$$v_j = \left(v_{jn} + V_{oFF}\right) > 0 \quad (9)$$

where j=a, b, c and v_{an}, v_{bn} and v_{cn} are defined in (1); whereas V_{oFF} is controlled by the neutral current i_n given by:

$$i_n = (i_a + i_b + i_c) \quad (10)$$

being i_a, i_b, i_c defined in (2). Hence, under steady-state conditions, $i_n = 0$ and V_{oFF} remains constant.

$$\begin{aligned} \langle i_a \rangle &= Ksin\left(\frac{\alpha_a}{2}\right)\left[n\left(v_b sin\left(\frac{\alpha_b}{2}\right)sin(\varphi_a - \varphi_b) + v_c sin\left(\frac{\alpha_c}{2}\right)sin(\varphi_a - \varphi_c)\right) - V_o sin\left(\frac{\alpha_o}{2}\right)sin(\varphi_a - \varphi_o)\right]; \\ \langle i_b \rangle &= Ksin\left(\frac{\alpha_b}{2}\right)\left[n\left(v_a sin\left(\frac{\alpha_a}{2}\right)sin(\varphi_b - \varphi_a) + v_c sin\left(\frac{\alpha_c}{2}\right)sin(\varphi_b - \varphi_c)\right) - V_o sin\left(\frac{\alpha_o}{2}\right)sin(\varphi_b - \varphi_o)\right]; \\ \langle i_c \rangle &= Ksin\left(\frac{\alpha_c}{2}\right)\left[n\left(v_a sin\left(\frac{\alpha_a}{2}\right)sin(\varphi_c - \varphi_a) + v_b sin\left(\frac{\alpha_b}{2}\right)sin(\varphi_c - \varphi_b)\right) - V_o sin\left(\frac{\alpha_o}{2}\right)sin(\varphi_c - \varphi_o)\right]; \end{aligned} \quad (11)$$

The PS angles $\varphi_a, \varphi_b, \varphi_c, \varphi_o$ and DR angles $\alpha_a, \alpha_b, \alpha_c, \alpha_o$ are calculated by a Newton-based optimization algorithm. Therefore, the average input currents $\langle i_a \rangle$, $\langle i_b \rangle$ and $\langle i_c \rangle$ in AC-side, for one switching period, are given by (11), being K a constant determined by the HF inductor value, n and f_s.

Note that the average currents given by (11) must match the grid currents given by (2). Therefore, this modulation involves high computational effort to calculate the command signals because of the non-linear dependence between the grid currents, the command signals, and the grid voltages.

For the above mentioned, this paper proposes a simpler modulation for the QAB AC-DC converter. Unlike the existing modulation, the resulting grid currents exhibit a low THD, and the command signals can be easily obtained with a low mathematical effort.

3. The Proposed Modulation

The proposed QAB AC-DC modulation is shown in Fig. 3.

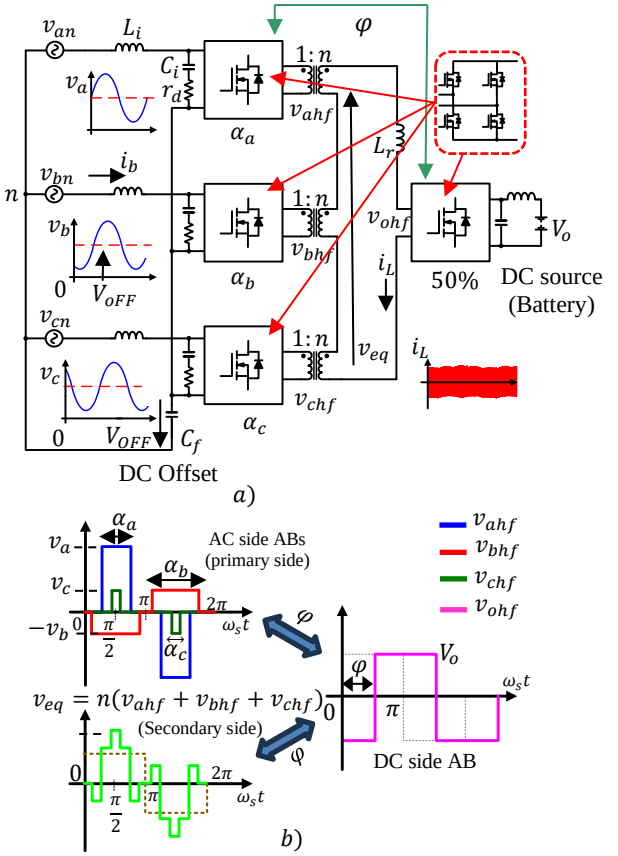

Fig. 3. The QAB AC-DC converter: (a) scheme (b) proposed modulation

In the proposed modulation, the offset grid voltages v_a, v_b and v_c, are modulated by symmetrical functions whose DR angles are given by α_a, α_b and α_c, whereas the DC source V_o is modulated by a 50% symmetrical function. The resulting HF voltages $v_{ahf}, v_{bhf}, v_{chf}$ and v_{ohf} are shown in in Fig. 3b. Note that v_{ohf} is phase-shifted φ with respect to v_{ahf}, v_{bhf} and v_{chf}.

Then, the average input currents $\langle i_a \rangle$, $\langle i_b \rangle$ and $\langle i_c \rangle$, in the AC-side, for one switching period, can be calculated as:

$$\begin{cases} \langle i_a \rangle = [K_L \sin(\varphi)] \sin\left(\frac{\alpha_a}{2}\right); \\ \langle i_b \rangle = [K_L \sin(\varphi)] \sin\left(\frac{\alpha_b}{2}\right); \\ \langle i_c \rangle = [K_L \sin(\varphi)] \sin\left(\frac{\alpha_c}{2}\right); \end{cases} \quad (12)$$

where:

$$K_L = \frac{8nV_o}{\pi^2 \omega_s L_r}$$

being n the turns-ratio relationship of the HF transformers, L_r is the HF inductance and ω_s is the switching frequency, which takes a constant value. Then, by comparing expressions (12) and (2), the PS angle φ and DRs angles can be calculated using (13) and (14), respectively.

$$\varphi = asin\left(\frac{I_m}{K_L}\right) \quad (13)$$

$$\begin{cases} \frac{\alpha_a}{2} = \omega_g t; \\ \frac{\alpha_b}{2} = \omega_g t - \frac{2\pi}{3}; \\ \frac{\alpha_c}{2} = \omega_g t + \frac{2\pi}{3}; \end{cases} \quad (14)$$

Therefore, the proposed modulation strategy enables straightforward parameter calculation compared to the approach presented in [7], resulting in a simpler modulation scheme.

Fig. 4 presents the simplified HF equivalent circuit of the QAB AC-DC converter. The AC-side HF voltages, expressed in Fourier series form, are given by:

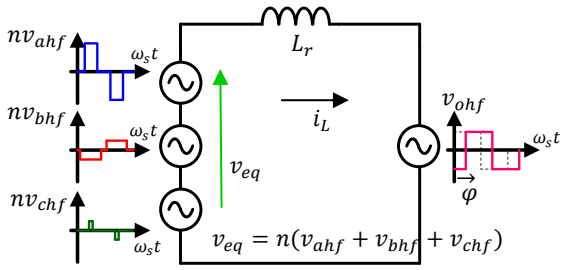

Fig. 4. The simplified HF equivalent circuit of the QAB AC-DC converter

$$v_{jhf} = v_{jn} \times \left[\sum_{k=1,35\ldots}^{\infty} \frac{4}{k\pi} \cos\left(k\left(\frac{\pi}{2} - \frac{\alpha_j}{2}\right)\right) \sin(k\omega_s t)\right] \quad (15)$$

where v_{jn} denotes the QAB voltage as defined in (9), and α_j is the DR for phase j, with j = a, b y c. The DC-side HF voltage, expressed in Fourier series form, is given by:

$$v_{ohf} = V_o \times \left[\sum_{k=1,35\ldots}^{\infty} \frac{4}{k\pi} \sin(k\omega_s t - \varphi)\right] \quad (16)$$

where V_o denotes the battery voltage.

$$\begin{aligned} i_{L(\omega_s)} &= \frac{4}{\pi \omega_s L_r}\left[V_o \cos(\omega_s t - \varphi) - \frac{3}{2} n V_m \cos(\omega_s t)\right] \\ i_{L(3\omega_s)} &= \frac{4}{9\pi \omega_s L_r}\left[V_o \cos(3\omega_s t - 3\varphi) + 3nV_{OFF} \sin(3\omega_g t) \cos(3\omega_s t)\right] \\ i_{L(5\omega_s)} &= \frac{4}{25\pi \omega_s L_r}\left[V_o \cos(5\omega_s t - 5\varphi) + \frac{3}{2} n V_m \cos(6\omega_g t) \cos(5\omega_s t)\right] \ldots \end{aligned} \quad (17)$$

The current i_L is given in (17), for the first three harmonics. Note that for the fundamental harmonic at ω_s, the current depends on φ. In contrast, the remaining harmonics present oscillations at low frequencies, multiples of the grid frequency ω_g, but their amplitudes are reduced progressively. Consequently, the QAB AC-DC converter design can be based on the fundamental harmonic at ω_s.

Therefore, to achieve an HF minimum current at the initial instant $\varphi = 0$, the DC- and AC-side voltage, the fundamental harmonic of the resulting modulated voltages, must match. Consequently, the transformer turns-ratio n are calculated by:

$$n = \frac{2V_o}{3V_m} \tag{18}$$

By substituting (18) into (13), the critical inductance L_{r-crit} for a PS angle of $\frac{\pi}{2}$ rad is obtained, as indicated in (19).

$$L_{r\_crit} = \frac{8V_o^2}{P_o \pi^2 \omega_s} \tag{19}$$

Therefore, the HF inductance L_r is selected below this value to ensure proper power transfer.

Moreover, to calculate the maximum HF current, the expression of i_L given in (17) is derived with respect to grid frequency $\omega_g t$. Then, the maximum occurs at $\omega_g t = (4k+1)\frac{\pi}{6}$, where the HF equivalent voltage v_{eq} (see Fig. 3) reaches its peak value.

4. QAB AC-DC DESIGN

The proposed modulation is validated by simulation and experimentally using the parameters described in Table I. First, $n = 0.86$ and $L_{r\_crit} = 122.9$ µH are calculated using (18) and (19) respectively. Since $L_r < L_{r\_crit}$, L_r is chosen in 109 μH. The AC filter and C_f are calculated as proposed in [9].

Table I. QAB AC-DC converter parameters

Item	Value	Item	Value
DC-Source Voltage and nominal Power (V_o, P_o)	400V, 1.4 kW	HF inductor L_r	109 μH
Grid Voltage (line - neutral)	220V RMS, 60 Hz	Turns-ratio HF transformers (1: n)	1: 0.86
Switching frequency (f_s)	120 kHz	LC Input Filter (L_i, C_i)	200μH, 1μF
OFFSET V_{oFF} and C_f	350V, 15μF	Damping resistor (r_d)	1.1Ω

With the previous considerations, a PS angle of 1.09 rad (62.5°) is calculated using (13). Hence, the HF current waveforms are obtained as a function of $\omega_g t$ variation within one switching period, as illustrated in Fig. 5. At 0 rad (0°), the waveform starts in state 1, as illustrated in Fig. 5a. Then, during $0 < \omega_g t < \frac{\pi}{6}$ rad to state 2, shown in Fig. 5b, until reaching the maximum at $\frac{\pi}{6}$ rad (30°) corresponding to state 3 in Fig. 5c. As $\omega_g t$ increases, the waveform returns to state 2 during $\frac{\pi}{6} < \omega_g t < \frac{\pi}{3}$ rad, and at $\frac{\pi}{3}$ rad (60°) returns to state 1. From $\frac{\pi}{3} < \omega_g t < \frac{\pi}{2}$ rad, the waveform operates in state 4, illustrated in Fig. 5d, and at $\frac{\pi}{2}$ rad (90°) in state 5, shown in Fig. 5e. Subsequently, from $\frac{\pi}{2} < \omega_g t < \frac{2\pi}{3}$ rad, the waveform returns to state 4, and finally, at $\frac{2\pi}{3}$ rad (120°), the waveform back to state 1. This sequence repeats with a periodicity of 120°. The maximum current, 7.6648 A, is observed when the HF equivalent voltage v_{eq} reaches the peak value (in 30°). Hence, the HF current varies with grid frequency and φ.

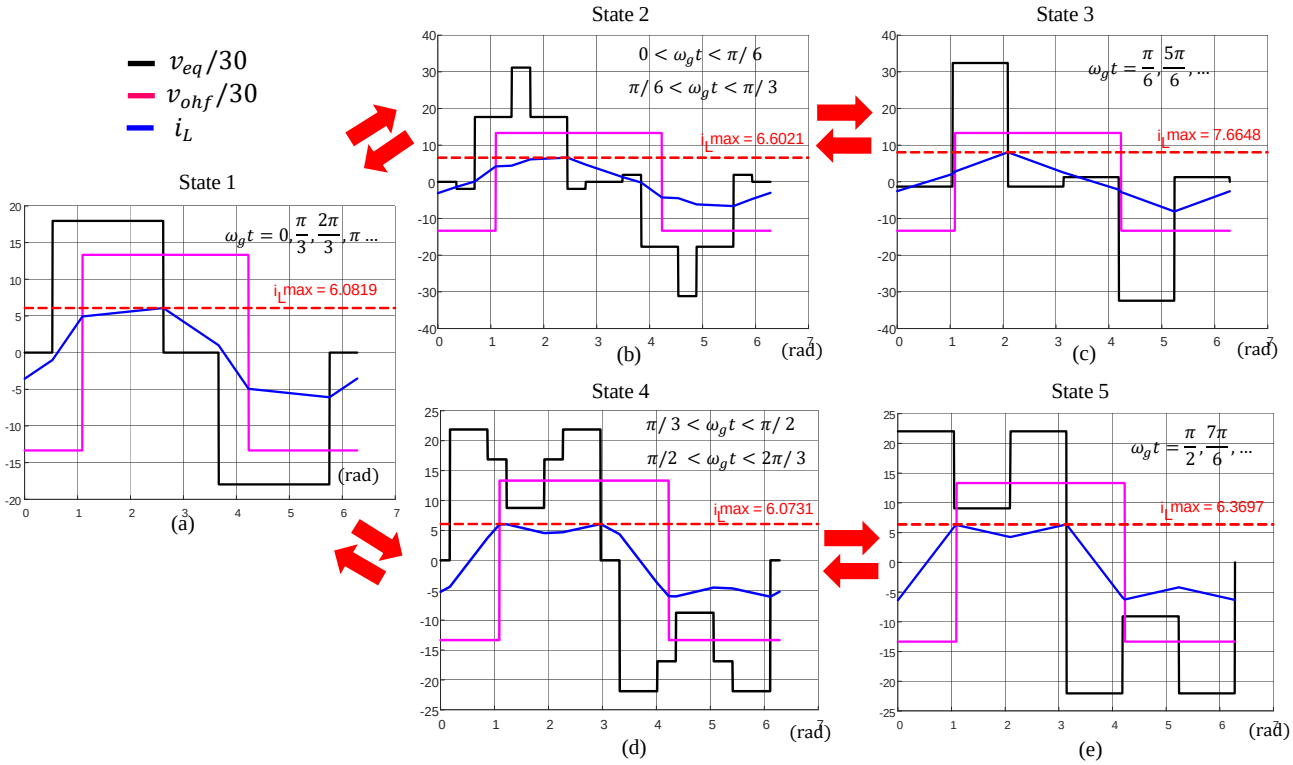

Fig. 5. Waveforms in i_L with respect to variations $\omega_g t$ in a switching periodo, for a PS angle of 62.5° (1.4 kW) (a) $\omega_g t = k\frac{\pi}{3}$ (b) $0 < \omega_g t < \frac{\pi}{6} \cup \frac{\pi}{6} < \omega_g t < \frac{\pi}{3}$ (c) $\omega_g t = (4k+1)\frac{\pi}{6}$ (d) $\frac{\pi}{3} < \omega_g t < \frac{\pi}{2} \cup \frac{\pi}{2} < \omega_g t < \frac{2\pi}{3}$ (e) $\omega_g t = (4k+3)\frac{\pi}{6}$

5. Simulation and Experimental Results

The simulation results for the nominal power and parameters indicated in Table I, are presented in Fig. 6. The resulting grid currents, one phase of the grid voltage, and the offset grid voltage are shown in Fig. 6a. Additionally, Fig. 6b shows the modulated offset grid voltage and the resulting HF current, considering three grid periods. Note that the HF current takes a quasi-constant amplitude throughout the grid period. Finally, Fig. 6c shows the resulting HF current over 4 switching periods. Note that the shape and amplitude of the HF current match with the analytically derived waveform shown in Fig. 5c.

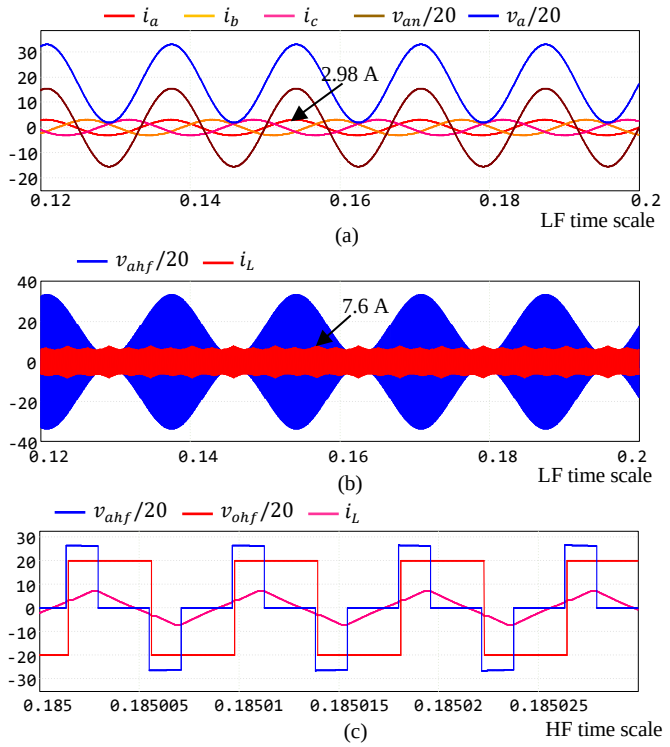

Fig. 6. Simulation results for 1.4 kW power at: (a) LF parameters (b) HF parameters (c) Over 4 switching periods

The experimental resulting grid current, for 1.4 kW power, is shown in Fig. 7. A very low THD (2.8%) was obtained. Similarly, the resulting modulated voltages and HF current, evaluated at $\omega_g t = 30°$, are shown in Fig. 8. Note that the waveform corresponds to Fig. 5c, validating the proposed modulation.

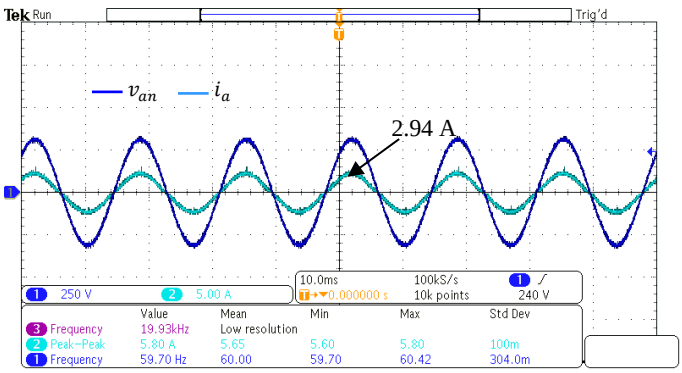

Fig. 7 Experimental results for 1.4 kW power at LF

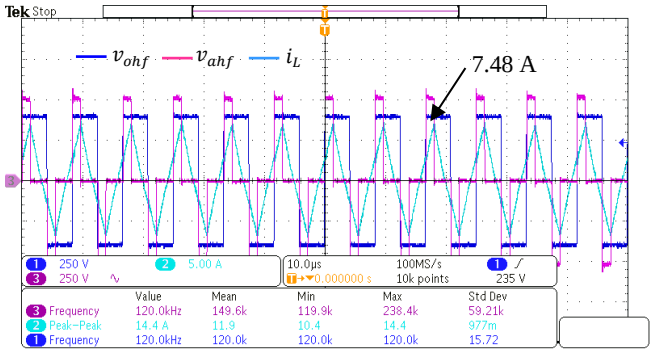

Fig. 8 Experimental results for 1.4 kW power at HF

6. Conclusions

A novel modulation for a single-stage three-phase QAB AC/DC converter has been introduced. In the proposed modulation, the command signals can be calculated with very low computation cost, compared to existing modulations. With the proposed modulation, the HF current presents a quasi-constant amplitude throughout the grid period. A low THD (2.8%) is obtained in the grid currents under open-loop operation. However, at low power, the THD is increased considerably. Hence, future work will focus on integrating a grid current control scheme into the proposed modulation strategy to address this limitation.

7. References

[1] H. Wouters and W. Martinez, "Bidirectional Onboard Chargers for Electric Vehicles: State-of-the-Art and Future Trends," in IEEE Transactions on Power Electronics, vol. 39, no. 1, pp. 693-716, Jan. 2024.

[2] N. D. Weise, G. Castelino, K. Basu and N. Mohan, "A Single-Stage Dual-Active-Bridge-Based Soft Switched AC–DC Converter With Open-Loop Power Factor Correction and Other Advanced Features," in IEEE Transactions on Power Electronics, vol. 29, no. 8, pp. 4007-4016, Aug. 2014.

[3] Y. -W. Cho, W. -J. Cha, J. -M. Kwon and B. -H. Kwon, "High-Efficiency Bidirectional DAB Inverter Using a Novel Hybrid Modulation for Stand-Alone Power Generating System With Low Input Voltage," in IEEE Transactions on Power Electronics, vol. 31, no. 6, pp. 4138-4147, June 2016.

[4] T. Chen, R. Yu and A. Q. Huang, "Variable-Switching-Frequency Single-Stage Bidirectional GaN AC–DC Converter for the Grid-Tied Battery Energy Storage System," in IEEE Transactions on Industrial Electronics, vol. 69, no. 11, pp. 10776-10786, Nov. 2022.

[5] J. Lu et al., "A Modular-Designed Three-Phase High-Efficiency High-Power-Density EV Battery Charger Using Dual/Triple-Phase-Shift Control," in IEEE Transactions on Power Electronics, vol. 33, no. 9, pp. 8091-8100, Sept. 2018.

[6] L. Schrittwieser, M. Leibl and J. W. Kolar, "99% Efficient Isolated Three-Phase Matrix-Type DAB Buck–Boost PFC Rectifier," in IEEE Transactions on Power Electronics, vol. 35, no. 1, pp. 138-157, Jan. 2020.

[7] B. J. D. Vermulst, J. L. Duarte, C. G. E. Wijnands and E. A. Lomonova, "Quad-Active-Bridge Single-Stage Bidirectional Three-Phase AC–DC Converter With Isolation: Introduction and Optimized Modulation," in IEEE Transactions on Power Electronics, vol. 32, no. 4, pp. 2546-2557, April 2017.

[8] H. Tao, A. Kotsopoulos, J. L. Duarte and M. A. M. Hendrix, "Transformer-Coupled Multiport ZVS Bidirectional DC–DC Converter With Wide Input Range," in IEEE Transactions on Power Electronics, vol. 23, no. 2, pp. 771-781, March 2008

[9] D. Sal y Rosas, D. Chavez and J. Tafur, "Quad-Active-Bridge Resonant-Type Single-Stage Three-Phase AC–DC Converter: Modulation and Control for V2G Applications," in *IEEE Transactions on Power Electronics*, vol. 40, no. 7, pp. 9034-9047, July 2025